

# Renormalized dispersion relations of $\beta$ -Fermi-Pasta-Ulam chains in equilibrium and nonequilibrium states

Shi-xiao W. Jiang,<sup>1</sup> Hai-hao Lu,<sup>1</sup> Douglas Zhou,<sup>1,\*</sup> and David Cai<sup>1,2,3,†</sup>

<sup>1</sup>*Department of Mathematics, MOE-LSC, and Institute of Natural Sciences, Shanghai Jiao Tong University, Shanghai 200240, China*

<sup>2</sup>*Courant Institute of Mathematical Sciences and Center for Neural Science, New York University, New York, New York 10012, USA*

<sup>3</sup>*NYUAD Institute, New York University Abu Dhabi, P.O. Box 129188, Abu Dhabi, United Arab Emirates*

(Received 19 April 2014; revised manuscript received 31 August 2014; published 30 September 2014)

We study the nonlinear dispersive characteristics in  $\beta$ -Fermi-Pasta-Ulam (FPU) chains in both thermal equilibrium and nonequilibrium steady state. By applying a multiple scale analysis to the FPU chain, we analyze the contribution of the trivial and nontrivial resonance to the renormalization of the dispersion relation. Our results show that the contribution of the nontrivial resonance remains significant to the renormalization, in particular, in strongly nonlinear regimes. We contrast our results with the dispersion relations obtained from the Zwanzig-Mori formalism and random phase approximation to further illustrate the role of resonances. Surprisingly, these theoretical dispersion relations can be generalized to describe dispersive characteristics well at the nonequilibrium steady state of the FPU chain with driving-damping in real space. Through numerical simulation, we confirm that the theoretical renormalized dispersion relations are valid for a wide range of nonlinearities in thermal equilibrium as well as in nonequilibrium steady state. We further show that the dispersive characteristics persist in nonequilibrium steady state driven-damped in Fourier space.

DOI: [10.1103/PhysRevE.90.032925](https://doi.org/10.1103/PhysRevE.90.032925)

PACS number(s): 05.45.-a, 63.20.D-, 05.40.-a, 52.25.Gj

## I. INTRODUCTION

Dispersive dynamics play an important role in characterizing many physical systems, e.g., atmosphere and ocean dynamics [1–4]. For linear dispersive waves, the dispersion relation, relating the wave frequency to the wave number, can be naturally defined [5–7]. However, in physical sciences and practical engineering, many systems are nonlinear and open to environment, i.e., they exchange energy or matter with their surroundings, such as waves in oceans [8–11] and in the atmosphere [12–14]. For these driven-damped nonlinear systems, it is natural to ask whether there exists a dispersion relation that can capture oscillation features of these waves. In this work, we focus on the  $\beta$ -Fermi-Pasta-Ulam (FPU) chain to investigate this question, in particular, that of how the linear dispersion relation becomes renormalized for nonlinearly interacting waves in both equilibrium and nonequilibrium.

The FPU lattice problem was first introduced to address the issues of energy equipartition and ergodicity in statistical physics [15]. The rich dynamics of the FPU system has motivated various mathematical and physical theories, such as the Kolmogorov–Arnol’d–Moser theorem and soliton theories [15–17]. It was found that when the total energy exceeds the so-called stochastic threshold, the FPU system becomes chaotic and eventually there is an energy equipartition in the system [18]. However, despite chaotic behaviors in thermal equilibrium, the  $\beta$ -FPU chain can still exhibit certain regular structures, such as the effective dispersive characteristics [19,20]. The wave-number–frequency spectral (WFS) analysis [21–23] is applied to confirm the existence of the dispersion relation of these turbulent waves. The dispersion relation obtained from the WFS method, referred to as the renormalized

dispersion relation, can deviate substantially from the linear dispersion. The renormalized dispersion relation was early numerically observed in Ref. [24] for the FPU chain in thermal equilibrium. Later, the dispersion relations were derived in Refs. [21,25] in the framework of the Zwanzig-Mori (ZM) projection [26,27]. It is demonstrated that the dispersive feature of those waves in thermal equilibrium can be induced by nonlinear wave-wave interactions, instead of inherited from their linear dispersive structures [19,21].

The study of resonance structures is one of the most important problems in wave turbulence theory [28–31]. In thermal equilibrium of the FPU chain, it is found that most of resonant interactions are trivial [19]. In our work, we demonstrate that both trivial and nontrivial quartet resonances play an important role in the renormalization of the dispersion relation by using a multiscale analysis [32,33]. We numerically examine the validity of predictions of the renormalized dispersion relation for a wide range of nonlinearities. Through the numerical simulation, we confirm our results regarding resonance structures in the renormalization of dispersion relations.

For the FPU system, the validity of the theoretical dispersion relations has been so far only examined in thermal equilibrium. As mentioned above, waves are often driven-damped systems. In this work, we further address two important questions: first, whether the dispersive characteristics of wave turbulence as manifested by an effective dispersive relation are still present for the FPU chain at a nonequilibrium steady state; second, if it exists, whether the dispersion relationship can be predicted theoretically for different scenarios of driving and dissipation.

We will answer the above questions in two settings for the FPU chain, one with driving-damping in real space and another with driving-damping in Fourier space. In the case of driving-damping in real space, we consider a  $\beta$ -FPU chain in contact with two Langevin heat baths interacting with particles at two ends [34,35]. We show that, for a wide

\*zdz@sjtu.edu.cn

†cai@cims.nyu.edu

range of driving strengths, there exists a dispersion relation obtained through the measurement using the WFS method. Our results further show that the measured dispersion relation is in excellent agreement with theoretical predictions of the renormalized dispersion relation. As will be seen below, the renormalization arises from the nonlinear wave interactions and is not a consequence of a frequency shift induced by the driving-damping as for a typical driven-damped linear system.

For the case of driving-damping in Fourier space, we consider a FPU chain driven at low  $k$  modes in the injection region and damped at high  $k$  modes in the dissipation region. For the weakly damped case, we find that our theoretical prediction of the renormalized dispersion relation can well capture the dispersive characteristics. However, for the strongly-damped case, the width of the dispersion spectrum becomes rather broad and theoretical predictions are no longer consistent with the measured dispersion relation given by the WFS method. However, these predictions are in qualitatively good agreement with the dispersion relation measured by the center of the dispersive band. For the broad band of spectrum, it seems that the dispersive characteristics may be better described by the center than by the peak of the band at a fixed  $k$  for the strongly damped case.

In this work, we have focused only on the renormalized dispersive behaviors of waves in the FPU system. However, we believe that the scenario of the renormalized dispersion relation may be extended to many other dispersive systems with general nonlinear and external interactions in both equilibrium and a driven-damped case.

This paper is organized as follows. In Sec. II, we consider the  $\beta$ -FPU chain in thermal equilibrium. We demonstrate that both trivial and nontrivial resonances contribute to the renormalization of the dispersion relation through a multiscale analysis. In Sec. III, we numerically study the dispersive characteristics of the FPU system in contact with two heat baths at the two ends. In Sec. IV, we investigate the dispersion relation for the  $k$ -space driven-damped FPU chain in the statistical steady state. In Sec. V, we present our conclusions and discussions. We relegate some technical points to Appendices. In particular, we present in Appendix A a derivation of the renormalized dispersion relation using the effective Lagrangian method.

## II. MULTISCALE ANALYSIS

We begin our investigation of the renormalized dispersion relation of the  $\beta$ -FPU chain by a multiple scale analysis. We consider the FPU chain of  $N$  particles with periodic boundary conditions. The system can be described by the Hamiltonian

$$H = \sum_{j=1}^N \frac{1}{2} p_j^2 + \frac{1}{2} (q_j - q_{j+1})^2 + \frac{\beta}{4} (q_j - q_{j+1})^4, \quad (1)$$

where  $p_j$  and  $q_j$  denote the momentum and the displacement of the  $j$ th particle, respectively, and the parameter  $\beta$  controls the strength of nonlinearity. In the Fourier space, the Hamiltonian can be written as

$$H = \sum_{k=0}^{N-1} \frac{1}{2} |P_k|^2 + \frac{1}{2} (\omega_k^{(0)})^2 |Q_k|^2 + V(Q), \quad (2)$$

where  $P_k$ ,  $Q_k$ , and  $V(Q)$  are the Fourier transforms of  $p_j$ ,  $q_j$ , and the quartic term in Hamiltonian (1), respectively. Here,  $\omega_k^{(0)}$  is the linear dispersion relation given by

$$\omega_k^{(0)} = 2 \sin\left(\frac{k\pi}{N}\right). \quad (3)$$

Note that the quantities appearing in above equations are all dimensionless. The corresponding dynamical equation to Hamiltonian (1) is

$$\begin{aligned} \ddot{q}_j - (q_{j+1} - 2q_j + q_{j-1}) \\ - \beta[(q_{j+1} - q_j)^3 - (q_j - q_{j-1})^3] = 0, \end{aligned} \quad (4)$$

where the overdot stands for the derivative with respect to time. Without loss of generality, in what follows, the zeroth mode of the displacement  $Q_0$  is set to zero, i.e.,  $\sum_{j=1}^N q_j = 0$ . The zeroth mode of the momentum  $P_0$  is also set to zero due to the fact that the total momentum can be set to zero, i.e.,  $\sum_{j=1}^N p_j = 0$ .

Next, we consider the FPU system (4) in the weakly nonlinear regime, i.e.,  $\beta \ll 1$ . To study the renormalization of waves, we seek an asymptotic expansion of displacement  $q_j$  and frequency  $\omega_k$  in powers of  $\beta$ ,

$$q_j = q_j^{(0)} + \beta q_j^{(1)} + O(\beta^2), \quad (5)$$

$$\omega_k = \omega_k^{(0)} + \beta \omega_k^{(1)} + O(\beta^2). \quad (6)$$

We proceed by substituting expansions (5) and (6) into the dynamical equation (4) and collecting terms in powers of  $\beta$  in order to determine  $\omega_k^{(0)}$  and  $\omega_k^{(1)}$ . At the leading order, the linear differential equation for  $q_j^{(0)}$  is obtained:

$$\ddot{q}_j^{(0)} - (q_{j+1}^{(0)} - 2q_j^{(0)} + q_{j-1}^{(0)}) = 0. \quad (7)$$

To investigate effects of nonlinear interactions among all modes  $k$ , we look for a multiwave solution with  $N-1$  components,

$$q_j^{(0)} = \frac{1}{\sqrt{N}} \sum_{k=1}^{N-1} \bar{Q}_k \exp(i\theta_{kj}), \quad (8)$$

where  $\bar{Q}_k$  is the amplitude of plane wave of the  $k$ th mode,  $\theta_{kj} = 2\pi k j / N - \omega_k t$  for  $k = 1, \dots, N-1$ . Substituting Eq. (8) into Eq. (7), we obtain the linear dispersion relation (3) of the leading frequency  $\omega_k^{(0)}$  [36,37]. At the next order, the terms proportional to  $\beta$  yield the equation for  $q_j^{(1)}$ ,

$$\begin{aligned} \ddot{q}_j^{(1)} - (q_{j+1}^{(1)} - 2q_j^{(1)} + q_{j-1}^{(1)}) \\ = 2\omega_k^{(0)} \omega_k^{(1)} q_j^{(0)} + [(q_{j+1}^{(0)} - q_j^{(0)})^3 - (q_j^{(0)} - q_{j-1}^{(0)})^3]. \end{aligned} \quad (9)$$

Because  $q_j^{(0)}$  satisfies Eq. (7), the fundamental harmonics  $\exp(i\theta_{kj})$  on the right-hand side of Eq. (9) are secular terms. After these secular terms are eliminated, the compatibility

condition that  $q_j^{(1)}$  is solvable from Eq. (9) gives rise to

$$\omega_k^{(1)} = \frac{3}{N} \left( \sum_{l=1}^{N-1} |\bar{Q}_l|^2 4 \sin^2 \frac{l\pi}{N} \right) \sin \frac{k\pi}{N} + \frac{1}{N} \sum_{\substack{l,m,s=1 \\ \text{nontrivial} \\ \text{resonant}}}^{N-1} \frac{\bar{Q}_l^* \bar{Q}_m \bar{Q}_s}{\bar{Q}_k} 4 \sin \frac{l\pi}{N} \sin \frac{m\pi}{N} \sin \frac{s\pi}{N}, \quad (10)$$

where the last summation  $\sum$  on the right-hand side only involves  $k, l, m, s$  that satisfy the nontrivial resonant condition:

$$k + l = m + s, \quad \omega_k^{(0)} + \omega_l^{(0)} = \omega_m^{(0)} + \omega_s^{(0)}. \quad (11)$$

Substituting Eqs. (3) and (10) into Eq. (6), we arrive at the approximation for frequency  $\omega_k$  to the second order of  $\beta$ ,

$$\omega_k^2 = (\omega_k^{(0)})^2 + \frac{3\beta}{N} \sum_{l=1}^{N-1} |\bar{Q}_l|^2 (\omega_l^{(0)})^2 (\omega_k^{(0)})^2 + \frac{\beta}{N} \sum_{\substack{l,m,s=1 \\ \text{nontrivial} \\ \text{resonant}}}^{N-1} \frac{\bar{Q}_m \bar{Q}_s \bar{Q}_l^*}{\bar{Q}_k} \omega_m^{(0)} \omega_s^{(0)} \omega_l^{(0)} \omega_k^{(0)} + O(\beta^2), \quad (12)$$

which can be expressed as

$$\omega_k^2 = \frac{\partial H^{\text{eff}} / \partial Q_k^*}{Q_k} + O(\beta^2) \quad (13)$$

by noting that  $Q_k = \bar{Q}_k \exp(-i\omega_k t)$ . Here  $H^{\text{eff}}$  is an effective Hamiltonian defined below and is not identical to the Hamiltonian (2):

$$H^{\text{eff}} = K + U + V^{\text{tr}} + V^{\text{nt}}, \quad (14)$$

where  $K, U$  are kinetic energy and quadratic potential energy, defined as

$$K = \frac{1}{2} \sum_{k=1}^{N-1} |P_k|^2, \quad U = \frac{1}{2} \sum_{k=1}^{N-1} (\omega_k^{(0)})^2 |Q_k|^2, \quad (15)$$

respectively. The quartic potential energies  $V^{\text{tr}}$  and  $V^{\text{nt}}$  contain only trivial resonant terms and nontrivial resonant terms, respectively:

$$V^{\text{tr}} = \frac{3\beta}{4N} \sum_{k,l=1}^{N-1} (\omega_k^{(0)})^2 (\omega_l^{(0)})^2 |Q_k|^2 |Q_l|^2, \quad (16)$$

$$V^{\text{nt}} = \frac{\beta}{4N} \sum_{\substack{k,l,m,s=1 \\ \text{nontrivial} \\ \text{resonant}}}^{N-1} \omega_k^{(0)} \omega_l^{(0)} \omega_m^{(0)} \omega_s^{(0)} Q_k^* Q_l^* Q_m Q_s. \quad (17)$$

From the definition of  $H^{\text{eff}}$  (14), it can be seen that not only the trivial resonance but also the nontrivial resonance contributes to the renormalization of the dispersion relation (13). In general, the dispersion relation (13) obtained from the multiple scale analysis is theoretically restricted to the weakly nonlinear regime. However, we will see below that its time averaged

version is a natural extension for the state of equilibrium and nonequilibrium and we will demonstrate through numerical simulation that it is not restricted to the weakly nonlinear limit.

To compare the results (13) with the dispersion relations in Refs. [21,25], we will briefly review various theoretical predictions of renormalized dispersion relations. In thermal equilibrium, the dispersion relation was obtained for the  $\beta$ -FPU chain from a linear Langevin equation via the Zwanzig-Mori (ZM) projection method [21,25]:

$$(\omega_k^L)^2 = \frac{\langle \frac{\partial H}{\partial Q_k^*} Q_k^* \rangle}{\langle |Q_k|^2 \rangle}, \quad (18)$$

where  $\langle \cdot \rangle$  denotes thermal average. By employing the energy equipartition theorem in Eq. (18),  $\omega_k^L$  can be written as [21]

$$\omega_k^N = \sqrt{\frac{\langle K \rangle}{\langle U \rangle}} \omega_k^{(0)}. \quad (19)$$

Based on the equality  $\langle K \rangle = \langle U \rangle + 2\langle V(Q) \rangle$  obtained from the equipartition theorem, Eq. (19) can be written in the form of  $\omega_k^N = \sqrt{1 + 2\langle V \rangle / \langle U \rangle} \omega_k^{(0)}$ , which has the same form as proposed in Refs. [24,38]. We will return below to discuss how Eq. (19) can be generalized in the nonequilibrium setting. In addition, through the application of random phase approximation (RPA) in Eq. (18), another theoretical renormalized dispersion was obtained as follows [20,21]:

$$(\omega_k^M)^2 = (\omega_k^{(0)})^2 \left( 1 + \frac{6\beta}{N} \langle U \rangle \right). \quad (20)$$

We note that the various approximations of the dispersion relation  $\omega_k^L$ ,  $\omega_k^N$ , and  $\omega_k^M$  are all obtained for the FPU chain in thermal equilibrium.

We now turn to the comparison of the renormalized dispersion relations mentioned above. We first discuss the relation between Eqs. (13) and (18). Multiplying  $Q_k^*$  and taking the thermal average for both numerator and denominator of Eq. (13), we can obtain the dispersion relation

$$\omega_k^2 = \frac{\langle \frac{\partial H^{\text{eff}}}{\partial Q_k^*} Q_k^* \rangle}{\langle |Q_k|^2 \rangle}, \quad (21)$$

which differs from Eq. (18) because  $H^{\text{eff}}$  is involved. The Hamiltonian  $H$  [Eq. (2)] possesses quartic terms of both resonant and nonresonant types, whereas  $H^{\text{eff}}$  [Eq. (14)] possesses quartic terms only of resonant type. However, the nonresonant terms have a total vanishing contribution in Eq. (18) because of the long-time average in thermal equilibrium [19]. Therefore,  $H^{\text{eff}}$  can be viewed as equivalent to  $H$  for long-time-averaged dynamics. That is, we can regard the dispersion relation  $\omega_k^L$  [Eq. (18)] as induced by resonance interactions only, including both trivial and nontrivial resonances, in the thermalized FPU chain. Incidentally, we point out that the Lagrangian approach [5] can be employed to obtain the renormalized dispersion relation  $\omega_k^L$  [Eq. (18)]. This derivation of  $\omega_k^L$  is presented in detail in Appendix A.

Next, we reveal the resonance structure that underlies the dispersion relation  $\omega_k^M$  (20) derived through the RPA. If the nontrivial resonance term  $V^{\text{nt}}$  in  $H^{\text{eff}}$  is neglected, the approximation for the renormalized frequency  $\omega_k$  [Eq. (12)] reduces to

$$\begin{aligned}\omega_k^2 &= (\omega_k^{(0)})^2 \left( 1 + \frac{3\beta}{N} \sum_{l=1}^{N-1} |\bar{Q}_l|^2 (\omega_l^{(0)})^2 \right) + O(\beta^2) \\ &= (\omega_k^{(0)})^2 \left( 1 + \frac{6\beta}{N} U \right) + O(\beta^2).\end{aligned}\quad (22)$$

We note that Eq. (22) is exactly the same as Eq. (20) upon taking the thermal average in the above dispersion relation (22) while ignoring higher order corrections  $O(\beta^2)$ . Therefore, the renormalized dispersion relation (20) takes into account only the trivial resonance with the nontrivial resonance neglected. This trivial resonance-induced frequency shift has been well discussed in the traditional weak turbulence theory [39]. As will be discussed below, it turns out that the nontrivial resonance also plays an important role in the renormalization of the dispersion relation.

To further understand the resonance contribution in the renormalization of the dispersion relation, we numerically study the FPU chain in thermal equilibrium. The chain was simulated with the parameters of  $N = 256$  and  $\beta = 100$  for a broad range of the energy  $H$ . Because the nonlinearity strength is controlled by the parameter  $\beta H$ , the larger  $H$  is, the stronger nonlinearity is when the parameter  $\beta$  is fixed. In order to compare with the theoretical predictions of the renormalized dispersion relation  $\omega_k^L$ ,  $\omega_k^N$ , and  $\omega_k^M$  in Eqs. (18), (19), and (20), respectively, we first need to obtain the numerically measured dispersion relation  $\Omega_k^{\text{meas}}$ . For a fixed mode  $k$ , the measured  $\Omega_k^{\text{meas}}$  is determined by the peak location of the spatiotemporal spectrum  $|\widehat{Q}_k(\omega)|^2$ , where  $\widehat{Q}_k(\omega)$  is the temporal Fourier transform of  $Q_k(t)$ . The quantities  $\langle \frac{\partial H}{\partial Q_k^*} Q_k^* \rangle$ ,  $\langle |Q_k|^2 \rangle$ ,  $\langle K \rangle$ , and  $\langle U \rangle$ , appearing in the renormalized dispersion relations  $\omega_k^L$ ,  $\omega_k^N$ , and  $\omega_k^M$ , are numerically computed by using a long-time average in thermal equilibrium instead of an ensemble average. The waves in the initial condition used in our simulation have their phases uniformly randomized [40] and we discard the initial transient in performing these time averages. Because our various predictions of the renormalized dispersion relation are proportional to the linear dispersion relation  $\omega_k^{(0)}$ , to compare these predictions, it is natural to define the renormalization factor

$$\eta_L = \frac{1}{N-1} \sum_{k=1}^{N-1} \tilde{\eta}_L(k), \quad (23)$$

$$\eta_N = \sqrt{\frac{\langle K \rangle}{\langle U \rangle}}, \quad (24)$$

$$\eta_M = \sqrt{1 + \frac{6\beta}{N} \langle U \rangle}, \quad (25)$$

where  $\tilde{\eta}_L(k)$  is the renormalization factor corresponding to the dispersion relation  $\omega_k^L$ ,

$$\tilde{\eta}_L(k) = \frac{\omega_k^L}{\omega_k^{(0)}}. \quad (26)$$

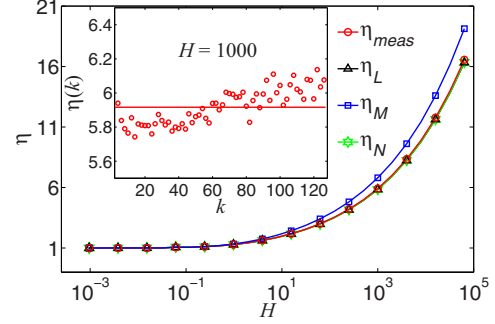


FIG. 1. (Color online) The renormalization factors as functions of the energy  $H$ . The chain was simulated using the parameters of  $N = 256$  and  $\beta = 100$ . Plotted is the renormalization factor  $\eta_{\text{meas}}$  [Eq. (27)] (red circles). For comparison, also plotted are the renormalization factors  $\eta_L$ ,  $\eta_N$ , and  $\eta_M$  from Eqs. (23), (24), and (25) with black triangles, green hexagons, and blue squares, respectively. It can be seen that  $\eta_{\text{meas}}$ ,  $\eta_L$ , and  $\eta_N$  almost overlap with each other. (Inset) Near- $k$  independence of the renormalization factors  $\tilde{\eta}_{\text{meas}}(k)$ . The red circles correspond to  $\tilde{\eta}_{\text{meas}}(k)$  for each mode  $k$ . The solid red line corresponds to the mean value  $\eta_{\text{meas}}$  [Eq. (27)].

To compare with the measured dispersion relation  $\Omega_k^{\text{meas}}$ , we also define the numerical renormalization factor  $\eta_{\text{meas}}$  by averaging the value of  $\tilde{\eta}_{\text{meas}}(k)$  over all modes  $k$ , i.e.,

$$\eta_{\text{meas}} = \frac{1}{N-1} \sum_{k=1}^{N-1} \tilde{\eta}_{\text{meas}}(k), \quad (27)$$

where

$$\tilde{\eta}_{\text{meas}}(k) = \frac{\Omega_k^{\text{meas}}}{\omega_k^{(0)}}. \quad (28)$$

The inset of Fig. 1 displays the renormalization factor  $\tilde{\eta}_{\text{meas}}(k)$  of each mode  $k$  (red circles) and its corresponding averaged renormalized factor  $\eta_{\text{meas}}$  (solid red line) for the case of  $H = 1000$ . It can be observed from Fig. 1 (inset) that the renormalized factor  $\tilde{\eta}_{\text{meas}}(k)$  is nearly independent of  $k$  with small variations of less than 3% around the mean value  $\eta_{\text{meas}}$ . Figure 1 displays the renormalization factors  $\eta_{\text{meas}}$ ,  $\eta_L$ ,  $\eta_N$ , and  $\eta_M$  as functions of the total energy  $H$ . It can be seen from Fig. 1 that the value of  $\eta_{\text{meas}}$  coincides with those of  $\eta_L$ ,  $\eta_N$ . The renormalized  $\omega_k^L$  and  $\omega_k^N$  are in excellent agreement with the measured dispersion relation  $\Omega_k^{\text{meas}}$  for a wide range of energy  $H$ . In contrast,  $\omega_k^M$  provides a less accurate approximation to  $\Omega_k^{\text{meas}}$ , but it can still capture the measured  $\Omega_k^{\text{meas}}$  quite well when the energy is not too large. We note that  $\omega_k^L$  and  $\omega_k^N$  have both trivial and nontrivial resonant contributions, whereas  $\omega_k^M$  has only the trivial resonant contribution. Therefore, we can conclude from Fig. 1 that the nontrivial resonance indeed contributes to the renormalization of dispersion relation although the majority of the contribution comes from trivial resonance at the thermal equilibrium of FPU chain. Here, it can be seen from Fig. 1 that the nontrivial resonance contribution becomes rather significant in strongly nonlinear regimes. Next, we will turn to the discussion about dispersive characteristics in the case of *nonequilibrium* steady state.

### III. $x$ -SPACE DRIVEN-DAMPED SYSTEM

We now address the main issue of whether the dispersive features of wave turbulence may still arise in nonequilibrium steady state for the system with two ends in contact with two thermal baths of different temperatures. The system will be referred to as an  $x$ -space driven-damped system. To be specific, we consider a one-dimensional system with the Hamiltonian

$$H' = \sum_{j=1}^N \frac{1}{2} p_j^2 + \sum_{j=1}^{N-1} \left[ \frac{1}{2} (q_j - q_{j+1})^2 + \frac{\beta}{4} (q_j - q_{j+1})^4 \right] + \left[ \frac{1}{2} q_1^2 + \frac{\beta}{4} q_1^4 \right] + \left[ \frac{1}{2} q_N^2 + \frac{\beta}{4} q_N^4 \right]. \quad (29)$$

The particles  $j = 1$  and  $j = N$  at the two ends are connected to Langevin thermal reservoirs; that is, the governing equations are given by

$$\dot{q}_1 = p_1, \quad \dot{p}_1 = -\frac{\partial H'}{\partial q_1} - \gamma_L p_1 + \sigma_L \xi_L(t), \quad (30a)$$

$$\dot{q}_j = p_j, \quad \dot{p}_j = -\frac{\partial H'}{\partial q_j}, \quad \text{for } j = 2, \dots, N-1, \quad (30b)$$

$$\dot{q}_N = p_N, \quad \dot{p}_N = -\frac{\partial H'}{\partial q_N} - \gamma_R p_N + \sigma_R \xi_R(t), \quad (30c)$$

where  $\xi_{L,R}(t)$  are independent Gaussian white noises, with  $\langle \xi_L(t) \rangle = 0$ ,  $\langle \xi_L(t) \xi_L(t') \rangle = \delta(t - t')$ , and  $\langle \xi_R(t) \rangle = 0$ ,  $\langle \xi_R(t) \xi_R(t') \rangle = \delta(t - t')$ . The driving coefficients  $\sigma_{L,R}$  characterize the driving strength and are linked to the dissipation coefficients  $\gamma_{L,R}$  by the fluctuation-dissipation theorem [27,41],  $\sigma_L^2 = 2\gamma_L k_B T_L$  and  $\sigma_R^2 = 2\gamma_R k_B T_R$ , where  $T_L, T_R$  are the temperatures of the left and right Langevin heat reservoirs, respectively.

We recall that the brackets  $\langle \cdot \rangle$  in the theoretical predictions  $\omega_k^L$ ,  $\omega_k^N$ , and  $\omega_k^M$  [Eqs. (18), (19), and (20), respectively], for the thermalized FPU chain, are interpreted as thermal average. In thermal equilibrium, the thermal average can be interpreted either as an ensemble average or as a long-time average if ergodicity holds for the system. In the nonequilibrium steady state of the FPU chain, the brackets  $\langle \cdot \rangle$  in Eqs. (18), (19), and (20) can no longer be interpreted as thermal average. A natural possibility is that the time average should be used instead. We note that the energy equipartition theorem is invoked in the derivation of Eq. (19) from Eq. (18) for the equilibrium case. What would be a possible theoretical counterpart in the transition from Eqs. (18) to (19) for the system in nonequilibrium steady state? In Appendix B, we outline an intuitive argument underlying the theoretical dispersion relation  $\omega_k^N$  [Eq. (19)] for nonequilibrium steady state when the time average is used for the bracket  $\langle \cdot \rangle$ . There, it can be seen that  $\omega_k^L$  and  $\omega_k^N$  are still closely related.

In what follows, we will investigate the theoretical possibility that, for the nonequilibrium steady state, these formulas of  $\omega_k^L$ ,  $\omega_k^N$ , and  $\omega_k^M$  remain valid if the brackets  $\langle \cdot \rangle$  are interpreted as a long-time average. An affirmative answer will clearly extend the validity of these predictions to the nonequilibrium steady state.

First, we numerically determine whether the renormalized dispersion relation persists for an  $x$ -space driven-damped FPU

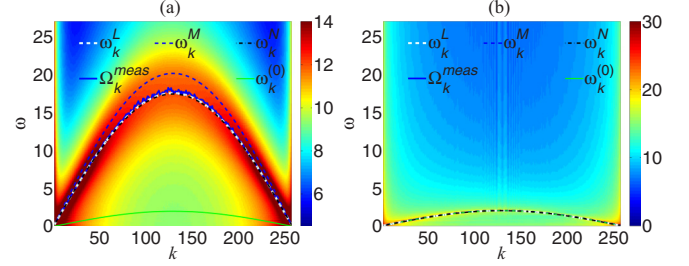


FIG. 2. (Color online) Comparison of renormalized dispersion relations for the  $x$ -space driven-damped  $\beta$ -FPU chain. The chain is simulated with the nonlinear strengths (a)  $\beta = 100$  and (b)  $\beta = 0$ . The other parameters of the chain are  $N = 256$ ,  $\sigma_L = 1$ ,  $\sigma_R = 10$ , and  $\gamma_L = \gamma_R = 1$ . Plotted is the logarithmic modulus  $\ln |\widehat{Q}_k(\omega)|^2$  by the WFS analysis with its magnitude color coded. The measured dispersion relation  $\Omega_k^{\text{meas}}$  is the location of the frequency peak of  $\ln |\widehat{Q}_k(\omega)|^2$  for each mode  $k$ . For comparison, also shown are  $\omega_k^L$  [Eq. (18)],  $\omega_k^M$  [Eq. (20)],  $\omega_k^N$  [Eq. (19)] and the linear dispersion relation  $\omega_k^{(0)}$  [Eq. (3)]. It can be seen in the left panel (a) that  $\omega_k^L$  and  $\omega_k^N$  almost overlap with each other and with  $\Omega_k^{\text{meas}}$ . It can also be observed in the right panel (b) that all the dispersion relations overlap with the linear dispersion relation.

system. In Fig. 2(a) the result of the  $\omega$ - $k$  analysis is displayed by the color coding of the logarithmic modulus,  $\ln |\widehat{Q}_k(\omega)|^2$ , where  $\widehat{Q}_k(\omega)$  is the temporal Fourier transform of  $Q_k(t)$ . The measured dispersion relation  $\Omega_k^{\text{meas}}$  [solid blue (dark gray) line] for the  $k$ th mode is determined by the peak location of the spectrum,  $|\widehat{Q}_k(\omega)|^2$ . It can be clearly seen in Fig. 2(a) that there is a dispersion relation, as indicated by the measured  $\Omega_k^{\text{meas}}$ . For comparison, also displayed are the theoretical predictions of renormalized dispersion relation  $\omega_k^L$ ,  $\omega_k^N$ , and  $\omega_k^M$ . It can be observed in Fig. 2(a) that the dispersion relations  $\omega_k^L$  (dashed white line),  $\omega_k^N$  (dash-dot black line), and  $\omega_k^M$  [dashed blue (dark gray) line] are good approximations to the measured  $\Omega_k^{\text{meas}}$ . It can be clearly seen that the renormalized dispersion relations  $\omega_k^L$  and  $\omega_k^N$  are both in excellent agreement with the measured  $\Omega_k^{\text{meas}}$ , whereas  $\omega_k^M$  is a fair approximation for the measured dispersion relation  $\Omega_k^{\text{meas}}$ . As discussed in Sec. II, the nontrivial resonant contribution is contained in the dispersion relations  $\omega_k^L$  and  $\omega_k^N$ , but neglected in the dispersion relation  $\omega_k^M$ . As seen in Fig. 2(a), this difference gives rise to the discrepancy between  $\omega_k^M$  and the measured  $\Omega_k^{\text{meas}}$ . Clearly, nontrivial resonance has an important effect also on the renormalization of the dispersion relation in nonequilibrium steady state.

Figure 2(b) displays the spectrum  $\ln |\widehat{Q}_k(\omega)|^2$  in the absence of nonlinearity (i.e.,  $\beta = 0$ ) with the same strengths of drivings and dampings as in Fig. 2(a). Here, we can see that all the dispersion relations coincide with the linear dispersion relation  $\omega_k^{(0)}$ . That is, the driving and damping essentially do not affect the oscillation frequency of each mode  $k$  significantly. Figure 2 clearly illustrates that the renormalization of the dispersion relation arises from the nonlinear wave interactions.

Our numerical results further show that, for a wide range of the driving strength  $\sigma_R$ , the measured  $\Omega_k^{\text{meas}}$  is observed and the theoretical predictions of the dispersion relation  $\omega_k^L$ ,  $\omega_k^N$ , and  $\omega_k^M$  are valid. The inset of Fig. 3 displays the renormalization factors  $\tilde{\eta}_{\text{meas}}(k)$  (circles) and  $\tilde{\eta}_L(k)$  (triangles)

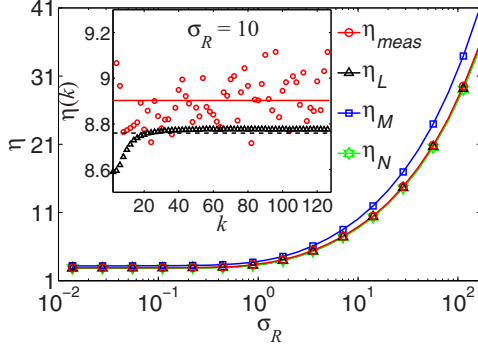


FIG. 3. (Color online) The renormalization factor as a function of driving strength  $\sigma_R$ . The chain was simulated with  $N = 256$ ,  $\beta = 100$ ,  $\sigma_L = 1$ , and  $\gamma_L = \gamma_R = 1$ . The renormalization factor  $\eta_{\text{meas}}$ ,  $\eta_L$ ,  $\eta_N$ , and  $\eta_M$  are depicted with red curve with circles, black curve with triangles, green curve with hexagons, and blue curve with squares, respectively. It can be observed that  $\eta_{\text{meas}}$ ,  $\eta_L$ , and  $\eta_N$  nearly overlap one another. (Inset) The renormalization factor  $\eta(k)$  versus wave number  $k$  for the system corresponding to that in Fig. 2(a). The parameter is  $\sigma_R = 10$ . The red circle corresponds to  $\tilde{\eta}_{\text{meas}}(k)$  in Eq. (28) and the black triangle corresponds to  $\tilde{\eta}_L(k)$  in Eq. (26). The solid red line and the dashed black line correspond to the mean values  $\eta_{\text{meas}}$  [Eq. (27)] and  $\eta_L$  [Eq. (23)], respectively.

for the driven-damped case which corresponds to the system in Fig. 2(a). It can be seen from Fig. 3 (inset) that  $\tilde{\eta}_{\text{meas}}(k)$  and  $\tilde{\eta}_L(k)$  are nearly independent of  $k$ . Their variations around the mean values  $\eta_{\text{meas}}$  (solid red line) and  $\eta_L$  (dashed black line) are very small and are less than 3% and 2%, respectively. To study the validity range of the theoretical prediction for dispersion relations in nonequilibrium steady state of the  $x$ -space driven-damped chain, we compare the renormalization factors for a wide range of  $\sigma_R$ . Figure 3 displays the renormalization factors  $\eta_{\text{meas}}$ ,  $\eta_L$ ,  $\eta_N$ , and  $\eta_M$  as a function of the driving strength  $\sigma_R$ , where  $\eta_{\text{meas}}$ ,  $\eta_L$ ,  $\eta_N$ ,  $\eta_M$  are defined in Eqs. (27), (23), (24), and (25), respectively. It can be seen from Fig. 3 that the measured renormalization factor  $\eta_{\text{meas}}$  becomes larger with stronger driving strength  $\sigma_R$ . It can be further observed that, for a wide range of  $\sigma_R$ , the theoretical predictions of the dispersion relation are in good agreement with the numerically measured one. Because, for large  $\sigma_R$ , the temperature is rather high at one side for the system, we can conclude that nonlinear effects play an increasingly important role in the renormalized behavior of dispersive waves as the driving force increases. Furthermore, the increasing discrepancy of  $\eta_{\text{meas}}$  and  $\eta_M$  as  $\sigma_R$  becomes larger shows that the nontrivial resonance contribution becomes increasingly important to the renormalized dispersion relation.

It is worthwhile to mention that we always verified that the system had reached steady state in our simulation before we used time average to compute the renormalized dispersion relations. We summarize the flux method used for the determination of the steady state of the systems in detail in Appendix C.

#### IV. $k$ -SPACE DRIVEN-DAMPED SYSTEM

We now turn to the issue of whether the dispersive characteristics persist in the nonequilibrium steady state of

the  $\beta$ -FPU chain driven at low  $k$  modes and damped at high  $k$  modes. We refer to this system as the  $k$ -space driven-damped FPU chain, in contrast to  $x$ -space driven-damped FPU chain in Sec. III. We consider the FPU chain with the Hamiltonian (2). The driving forces are imposed at low  $k$  modes while the damping forces are imposed at high  $k$  modes. Thus, the  $k$ -space driven-damped system is described as follows:

$$\dot{Q}_{k_l} = P_{k_l}, \quad \dot{P}_{k_l} = -\frac{\partial H}{\partial Q_{k_l}^*} + \sigma \xi_{k_l}(t) \quad (31a)$$

for a low driven mode  $k_l$  in the injection range  $\mathcal{K}_L$ ,

$$\dot{Q}_{k_m} = P_{k_m}, \quad \dot{P}_{k_m} = -\frac{\partial H}{\partial Q_{k_m}^*} \quad (31b)$$

for a mode  $k_m$  in the inertial range  $\mathcal{K}_M$ , and

$$\dot{Q}_{k_h} = P_{k_h}, \quad \dot{P}_{k_h} = -\frac{\partial H}{\partial Q_{k_h}^*} - \gamma P_{k_h} \quad (31c)$$

for a high mode  $k_h$  in the dissipation range  $\mathcal{K}_H$ , where  $\xi_{k_l}(t)$  is the independent Gaussian white noise, with zero mean and  $\langle \xi_{k_l}(t) \xi_{k_l}(t') \rangle = \delta(t - t')$  for  $k_l \in \mathcal{K}_L$ ,  $\sigma$  is a driving coefficient for all driven modes  $k_l \in \mathcal{K}_L$ , and  $\gamma$  is the damping coefficient for all damped modes  $k_h \in \mathcal{K}_H$ . The number of driven modes is denoted by  $n_{dv}$  and the number of damped modes is denoted by  $n_{dp}$ .

We study the system (31) in two regimes: one is a weakly damped regime and the other is a strongly damped regime. From our numerical study, it turns out that these two regimes possess similar dispersive behaviors of waves. However, they differ in many important aspects as will be discussed below. We first verify the existence of the renormalized dispersive relation for the FPU chain in the weakly-damped regime. Figure 4(a) displays the measured dispersion relation  $\Omega_k^{\text{meas}}$  in comparison with the theoretical renormalized dispersion relations  $\omega_k^L$ ,  $\omega_k^N$ , and  $\omega_k^M$ , respectively. Here, the theoretical  $\omega_k^L$ ,  $\omega_k^N$ , and  $\omega_k^M$  are still in the form of Eqs. (18), (19), and (20), respectively, but  $\langle \cdot \rangle$  in them are again interpreted as a long-time average as in Sec. III. From Fig. 4(a), it can be again observed that there is a good agreement between numerically measured  $\Omega_k^{\text{meas}}$  and theoretical predictions for the renormalized dispersion relation. As in the case of thermal equilibrium and the  $x$ -space driven-damped system,  $\omega_k^L$  and  $\omega_k^N$  capture  $\Omega_k^{\text{meas}}$  better than  $\omega_k^M$ .

However, in the strongly damped case, the dispersive characteristics become rather different. Figure 4(b) shows an example of the strongly damped regime. Here, the measured dispersion relation  $\Omega_k^{\text{meas}}$  no longer possesses a strong dispersion characteristics as in the weakly damped case. For a mode  $k$  in the inertial range  $\mathcal{K}_M$ , the width of the dispersion peak now is rather broad and the measured  $\Omega_k^{\text{meas}}$  no longer closely coincides with theoretical predictions  $\omega_k^L$ ,  $\omega_k^N$ , or  $\omega_k^M$ . However, it turns out that these theoretical predictions are in qualitatively good agreement with the center of the dispersive band as indicated in Fig. 4(b), where the center is defined as

$$\Omega_k^c = \frac{\int \omega |\widehat{Q}_k(\omega)|^2 d\omega}{\int |\widehat{Q}_k(\omega)|^2 d\omega}. \quad (32)$$

For a broad peak, the center  $\Omega_k^c$  may be a better representation of the band than the peak location  $\Omega_k^{\text{meas}}$ , as can be seen in Fig. 4(b). Incidentally, it is worth mentioning that we also

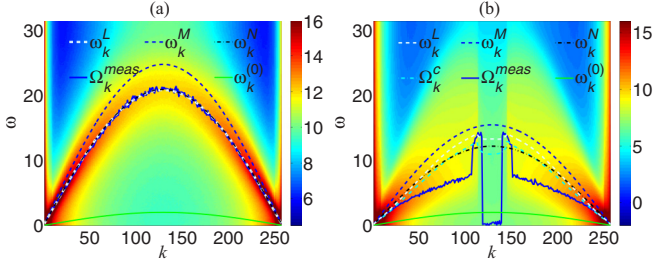


FIG. 4. (Color online) Comparison of renormalized dispersion relations for the  $k$ -space driven-damped  $\beta$ -FPU chain. The left panel (a) displays the renormalized dispersion relations of the  $\beta$ -FPU chain for the weakly damped case. The parameters are  $N = 256$ ,  $\beta = 100$ ,  $\sigma = 2$ ,  $\gamma = 0.1$ ,  $n_{dv} = 16$ , and  $n_{dp} = 16$ . The right panel (b) displays the dispersion relations for the strongly damped  $\beta$ -FPU chain with the parameters  $N = 256$ ,  $\beta = 100$ ,  $\sigma = 2$ ,  $\gamma = 10$ ,  $n_{dv} = 16$ , and  $n_{dp} = 32$  (note that more damping modes are used here than in (a), in addition to the stronger damp coefficient, for this strongly damped case). The spatiotemporal spectrum  $\ln|\widehat{Q}_k(\omega)|^2$  is plotted with its value color-coded; its corresponding peak  $\Omega_k^{\text{meas}}$  is the measured dispersion relation. Also plotted are the theoretical predictions for the renormalizations  $\omega_k^L$  [Eq. (18)],  $\omega_k^M$  [Eq. (20)],  $\omega_k^N$  [Eq. (19)], and linear dispersion relation  $\omega_k^{(0)}$  [Eq. (3)]. Note that  $\omega_k^L$ ,  $\omega_k^N$  nearly overlap with  $\Omega_k^{\text{meas}}$  in the left panel (a). The right panel (b) displays the center of the dispersive band  $\Omega_k^c$  [Eq. (32)] with the dash-dot cyan (light gray) curve.

monitored our numerical simulation so as to ensure our results are obtained from a steady state.

Next, we make an attempt to understand the reason for the different behaviors of dispersive waves in these two regimes. As is expected, the dispersive characteristics of a near-equilibrium system could be very similar to that of an equilibrium system. Our numerical measurement of the kinetic energy indeed indicates that the weakly damped system is near equilibrium whereas the strongly damped system is far from equilibrium. Figures 5(a) and 5(b) display the kinetic energy  $\langle |P_k|^2 \rangle$  for the systems corresponding to Figs. 4(a) and 4(b), respectively, where the bracket  $\langle \cdot \rangle$  denotes the long-time average. Clearly, in thermal equilibrium, the kinetic energy  $\langle |P_k|^2 \rangle$  is equal among all modes  $k$  due to energy equipartition. In the weakly damped case [Fig. 5(a)], the maximum value of the kinetic energy is estimated to be 8% larger than the minimum value in the inertial range  $\mathcal{K}_M$ . However, this ratio becomes much larger and is about 37% in the strongly damped

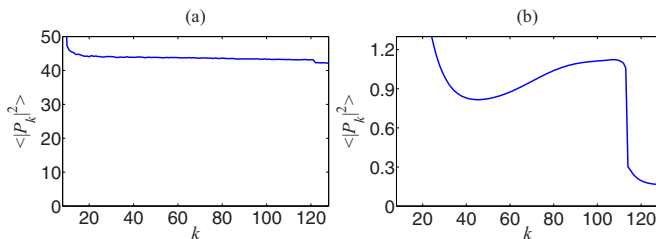


FIG. 5. (Color online) The kinetic energy  $\langle |P_k|^2 \rangle$  for modes  $k$  in the inertial range for (a) the weakly damped and (b) the strongly damped FPU chain whose spatiotemporal spectrum is shown in Figs. 4(a) and 4(b), respectively.

case [Fig. 5(b)]. As indicated by this ratio, the weakly damped system is much closer to an equilibrium system than the strongly damped system.

To further quantify whether a  $k$ -space driven-damped system is near equilibrium or not, we investigate how close the distribution of the real part of  $P_k$ ,  $\text{Re}(P_k)$ , is to the Gaussian distribution for the modes in the inertial range. The distribution of  $\text{Re}(P_k)$  should be nearly Gaussian for a near-equilibrium FPU chain as can be seen from the momentum part of Boltzmann factor. We examine the distribution by computing the ratio of central moments  $\bar{r}_4, \bar{r}_6, \bar{r}_8$ :

$$\begin{aligned} r_4(k) &= \frac{\langle R_k^4 \rangle}{\langle R_k^2 \rangle^2}, & \bar{r}_4 &= \frac{1}{N - n_{dv} - n_{dp}} \sum_{k \in \mathcal{K}_M} r_4(k), \\ r_6(k) &= \frac{\langle R_k^6 \rangle}{\langle R_k^2 \rangle^3}, & \bar{r}_6 &= \frac{1}{N - n_{dv} - n_{dp}} \sum_{k \in \mathcal{K}_M} r_6(k), \\ r_8(k) &= \frac{\langle R_k^8 \rangle}{\langle R_k^2 \rangle^4}, & \bar{r}_8 &= \frac{1}{N - n_{dv} - n_{dp}} \sum_{k \in \mathcal{K}_M} r_8(k), \end{aligned} \quad (33)$$

where  $R_k = \text{Re}(P_k) - \langle \text{Re}(P_k) \rangle$ . For the weakly damped case, we find that these ratios ( $\bar{r}_4 = 3.02$ ,  $\bar{r}_6 = 15.3$ , and  $\bar{r}_8 = 109.0$ ) have very small deviations from the corresponding values for the Gaussian distribution ( $\bar{r}_4 = 3$ ,  $\bar{r}_6 = 15$ , and  $\bar{r}_8 = 105$ ). Therefore, the weakly damped system can be viewed as a near-equilibrium system. In contrast, for the strongly damped case, the distribution of  $\text{Re}(P_k)$  is far from Gaussian ( $\bar{r}_4 = 3.29$ ,  $\bar{r}_6 = 19.9$ , and  $\bar{r}_8 = 187.5$ ), and hence this system is far away from equilibrium.

Incidentally, we also have computed these moment ratios for the  $x$ -space driven-damped FPU system in Fig. 2(a) ( $\bar{r}_4 = 2.97$ ,  $\bar{r}_6 = 14.6$ , and  $\bar{r}_8 = 99.1$ ). In that case, the distribution of  $\text{Re}(P_k)$  is nearly Gaussian. In addition, we also have numerically verified that  $\langle |P_k|^2 \rangle$  are equal for all Fourier modes. However, the system is away from equilibrium as can be confirmed by the kinetic energy profile  $\langle p_j^2 \rangle$  [Fig. 7(b)] in Appendix C. (In equilibrium, the kinetic energy profile should be independent of the location by the equipartition theorem from the Boltzmann distribution). In this case, it appears that if  $P_k$  is nearly Gaussian, the renormalized dispersion relations can be well captured by our theoretical predictions. It is important to systematically investigate this possibility theoretically in the future for various dynamical scenarios of driving and dissipation.

In summary, the dispersive characteristics can still persist and those theoretical dispersion relations are valid in predicting the measured  $\Omega_k^{\text{meas}}$  in the  $k$ -space weakly damped FPU chain in near equilibrium. However, for a strongly damped case, because the chain is far from equilibrium and  $P_k$  strongly deviates from Gaussianity, the dispersive structures are no longer as prominent as those in the near-equilibrium situation. In this regime, our theoretical results can only qualitatively describe the dispersive characteristics.

## V. CONCLUSIONS AND DISCUSSIONS

We have applied a multiple scale analysis to study the renormalization of the dispersion relation in the  $\beta$ -FPU chain with periodic boundary conditions. We have theoretically

shown both trivial resonances  $V^{\text{tr}}$  and nontrivial resonances  $V^{\text{nt}}$  contribute to the renormalized dispersion  $\omega_k^L$  and  $\omega_k^N$ , whereas there are only trivial resonance contributions in  $\omega_k^M$ . This clarifies the contributions of various resonant structures in these renormalized dispersion relations that have appeared in previous literature. For the FPU chain in thermal equilibrium,  $\omega_k^L$  and  $\omega_k^N$  are shown to be in much better agreement with the measured  $\Omega_k^{\text{meas}}$  than  $\omega_k^M$  for a wide range of nonlinearity strengths. For an  $x$ -space driven-damped FPU chain, we have demonstrated that the renormalized dispersion relation again arises as a consequence of the nonlinear wave interactions. The renormalization of the dispersion relation also comes from the contribution of both trivial and nontrivial resonant interactions. For the nonequilibrium steady state of a  $k$ -space driven-damped  $\beta$ -FPU chain, if the damping is weak in the dissipation region, dispersive characteristics are still strong and can be well captured by our theoretical predictions. However, for the  $k$ -space strongly damped case, the theoretical predictions can only provide a qualitatively good approximation to the center of the dispersive band  $\Omega_k^c$ . We have also examined possible underlying reasons for this contrast between the weakly damped and the strongly damped cases, and point out a possible connection between the near Gaussianity of  $P_k$  and the validity of our theoretical predictions for renormalized dispersion relations.

Finally, we briefly discuss the renormalization of dispersion relations in thermal equilibrium for a purely quartic chain [38] with the Hamiltonian  $H = \sum_{j=1}^N \frac{1}{2} p_j^2 + \frac{\beta}{4} (q_j - q_{j+1})^4$ . In this case, the linear dispersion relation is absent and the multiscale analysis is not applicable. However, the phenomenon of the renormalized dispersion relation still persists in thermal equilibrium [Fig. 6(a)]. Furthermore, it can be seen from Fig. 6(b) that the value of renormalization factor  $\eta_{\text{meas}}$  is in excellent agreement with those of  $\eta_L$  and  $\eta_N$  for a wide range

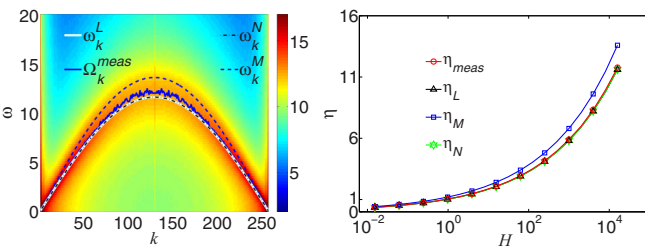


FIG. 6. (Color online) (a) The renormalized dispersion relations for the purely quartic chain in thermal equilibrium. The chain was simulated with  $N = 256$ ,  $\beta = 100$ , and  $H = 1000$ . Plotted is the measured dispersion relation  $\Omega_k^{\text{meas}}$  [solid blue (dark gray) curve]. For comparison, also plotted are the theoretical predictions for the renormalized dispersion relations  $\omega_k^L$  [Eq. (18)] (solid white curve),  $\omega_k^M$  [Eq. (20)] (dashed blue curve), and  $\omega_k^N$  [Eq. (19)] (dash-dot black curve). Note that  $\omega_k^L$  and  $\omega_k^N$  nearly overlap with each other. (b) The renormalization factors as a function of the energy  $H$  for purely quartic chains. The chain was simulated using the parameters of  $N = 256$  and  $\beta = 100$ . Plotted is the renormalization factor  $\eta_{\text{meas}}$  [Eq. (27)] (red circles). For comparison, also plotted are the renormalization factors  $\eta_L$ ,  $\eta_N$ , and  $\eta_M$  from Eqs. (23), (24), and (25) with black triangles, green hexagons, and blue squares, respectively. Note that  $\eta_{\text{meas}}$ ,  $\eta_L$ , and  $\eta_N$  nearly overlap with each other.

of  $H$  in thermal equilibrium. As a natural extension of the above results, it is interesting to study the renormalization of dispersion relations for a purely quartic chain in the nonequilibrium steady state case in future work.

## ACKNOWLEDGMENTS

D.Z. is supported by the Shanghai Pujiang Program (Grant No. 10PJ1406300) and National Science Foundation in China (Grants No. NSFC-11101275 and No. 91230202), and D.C. is supported by Grant No. NSF-DMS-1009575. S.J, D.Z., and D.C. are supported by the NYU Abu Dhabi Research Institute Grant No. G1301, and H.L. is supported by the Zhiyuan College Undergraduate Research Program at Shanghai Jiao Tong University.

## APPENDIX A: THE DERIVATION OF $\omega_k^L$ [Eq. (18)] THROUGH THE LAGRANGIAN METHOD

The Lagrangian for the  $\beta$ -FPU chain is

$$L = \sum_{j=1}^N \frac{1}{2} \dot{q}_j^2 - \left( \frac{1}{2} (q_j - q_{j+1})^2 + \frac{\beta}{4} (q_j - q_{j+1})^4 \right) \equiv T - W, \quad (\text{A1})$$

where  $T$  is the total kinetic energy and  $W$  is the total potential energy,

$$T = \sum_{j=1}^N \frac{1}{2} \dot{q}_j^2, \quad W = \sum_{j=1}^N \left( \frac{1}{2} (q_j - q_{j+1})^2 + \frac{\beta}{4} (q_j - q_{j+1})^4 \right). \quad (\text{A2})$$

After we substitute the multiwave expansion (8) into Eq. (A1), the Lagrangian becomes,

$$L = \sum_{k=1}^{N-1} \frac{1}{2} \omega_k^2 |\bar{Q}_k|^2 - W(\bar{Q}). \quad (\text{A3})$$

The vanishing variation of Eq. (A3) with respect to  $\bar{Q}_k^*$  yields the equation,  $\omega_k^2 \bar{Q}_k - \partial H / \partial \bar{Q}_k^* = 0$ , where  $H = K + W$ , and  $K$  is defined in Eq. (15). Hence, the dispersion relation is

$$\omega_k^2 = \frac{\partial H / \partial Q_k^*}{Q_k}, \quad (\text{A4})$$

by noting that  $Q_k = \bar{Q}_k \exp(-i\omega_k t)$ . After multiplying  $Q_k^*$  and taking the thermal average for the numerator and denominator of Eq. (A4), we can obtain exactly the same dispersion relation as  $\omega_k^L$  in Eq. (18). In general, the Lagrangian method is theoretically restricted to a weakly nonlinear regime typical as a multiscale method. However, in the derivation of dispersion relation (A4), we have not explicitly invoked the weak nonlinearity assumption. It appears that the Lagrangian method can be extended to a fully nonlinear regime to derive the effective dispersion relation in the case of the thermalized FPU chain. Our numerical results provide support to this observation, as can be seen in the main text.

### APPENDIX B: THE DERIVATION OF $\omega_k^N$ FOR THE $x$ -SPACE DRIVEN-DAMPED FPU CHAIN

Here, we present an intuitive argument linking the dispersion relation  $\omega_k^N$  (19) to  $\omega_k^L$  (18) in the nonequilibrium steady state of an  $x$ -space driven-damped system under the assumption that  $\tilde{\eta}_N(k)$  is independent of mode  $k$ , where

$$\tilde{\eta}_N^2(k) \equiv \langle \frac{1}{2} |P_k|^2 \rangle / \langle \frac{1}{2} (\omega_k^{(0)})^2 |Q_k|^2 \rangle. \quad (\text{B1})$$

For the nonequilibrium steady state, the dispersion relation  $\omega_k^N$  [Eq. (19)] cannot be directly derived from  $\omega_k^L$  by using the energy equipartition theorem since the theorem no longer holds. First, we can prove the validity of the equality

$$\langle \dot{Q}_k^* P_k \rangle = -\langle Q_k^* \dot{P}_k \rangle \quad (\text{B2})$$

by using integration by parts,

$$\begin{aligned} \langle \dot{Q}_k^* P_k \rangle &= \frac{1}{T} \int_0^T \dot{Q}_k^* P_k dt = \frac{1}{T} Q_k^* P_k |_0^T - \frac{1}{T} \int_0^T Q_k^* \dot{P}_k dt \\ &= \frac{1}{T} Q_k^* P_k |_0^T - \langle Q_k^* \dot{P}_k \rangle = -\langle Q_k^* \dot{P}_k \rangle, \end{aligned}$$

where the term  $\frac{1}{T} Q_k^* P_k |_0^T$  vanishes for sufficiently large time  $T$  if  $Q_k^* P_k$  is assumed to be bounded for large times. Then the dispersion relation  $\omega_k^L$  reduces to

$$\begin{aligned} (\omega_k^L)^2 &= \frac{\langle Q_k^* \frac{\partial H}{\partial Q_k} \rangle}{\langle |Q_k|^2 \rangle} = \frac{\langle Q_k^* (-\dot{P}_k + \sigma \hat{\xi}_k - \gamma \hat{P}_k) \rangle}{\langle |Q_k|^2 \rangle} \\ &= \frac{-\langle Q_k^* \dot{P}_k \rangle}{\langle |Q_k|^2 \rangle} = \frac{\langle \dot{Q}_k^* P_k \rangle}{\langle |Q_k|^2 \rangle} = \frac{\langle |P_k|^2 \rangle}{\langle |Q_k|^2 \rangle}, \end{aligned} \quad (\text{B3})$$

where  $\sigma \hat{\xi}_k = \mathcal{F}\{(\sigma_L \xi_L, 0, \dots, 0, \sigma_R \xi_R)\}$  and  $\gamma \hat{P}_k = \mathcal{F}\{(\gamma_L p_1, 0, \dots, 0, \gamma_R p_N)\}$ , respectively. Here  $\mathcal{F}\{\cdot\}$  denotes the Fourier transform. It can be shown that  $\langle \sigma \hat{\xi}_k Q_k^* \rangle$  vanishes and we have numerically examined that  $\gamma \hat{P}_k$  are nearly orthogonal to  $Q_k^*$ . If the renormalized factor  $\tilde{\eta}_N(k)$  is independent of  $k$ , from (B3) we can easily obtain the dispersion relation  $\omega_k^N$  [Eq. (19)].

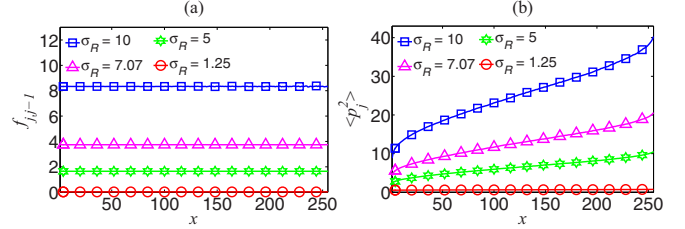


FIG. 7. (Color online) (a) The energy flux  $f_{j,j-1}$  [Eq. (C1)] and (b) the kinetic energy  $\langle p_j^2 \rangle$  for various driving strengths  $\sigma_R$  corresponding to the systems in Fig. 3. The simulation for the  $\beta$ -FPU chain is performed with parameters of  $N = 256$ ,  $\beta = 100$ ,  $\gamma_L = \gamma_R = 1$ , and  $\sigma_L = 1$ . The blue line with squares, magenta line with triangles, green line with hexagons and red line with circles correspond to (a) the flux profile and (b) the kinetic energy profile for the system with driving strengths  $\sigma_R$  of 10, 7.07, 5 and 1.25, respectively.

### APPENDIX C: THE FLUX IN THE NONEQUILIBRIUM STEADY STATE OF AN $x$ -SPACE DRIVEN-DAMPED FPU CHAIN

In order to study the renormalized dispersion, we need to verify that the system reaches its steady state. In the nonequilibrium steady state, clearly the energy flux is constant over space [34,35]. In this system (30), the flux  $f_{j,j-1}$  is

$$f_{j,j-1} = \langle p_j [(q_j - q_{j-1}) + \beta (q_j - q_{j-1})^3] \rangle, \quad (\text{C1})$$

where the bracket  $\langle \cdot \rangle$  stands for the long-time average. Figure 7(a) displays the energy flux  $f_{j,j-1}$  corresponding to some cases in Fig. 3. There is an equality on all  $f_{j,j-1}$  for  $j = 2, \dots, N$  from Fig. 7(a). This is indicative that these systems have converged to the steady state. Figure 7(b) displays the corresponding kinetic energy  $\langle p_j^2 \rangle$ . It can be seen from Fig. 7(b) that the kinetic energy profile becomes steeper when the temperature at the right end becomes higher. We note that the kinetic energy is shared equally among all  $\langle p_j^2 \rangle$  for the FPU chain in thermal equilibrium. As expected, the system deviates from thermal equilibrium as the temperature at one side increases.

- 
- [1] R. M. Jones, *J. Geophys. Res.* **110**, D22106 (2005).  
[2] J. P. Dugan, H. H. Suzukawa, C. P. Forsyth, and M. S. Farber, *IEEE Trans. Geosci. Remote Sens.* **34**, 1282 (1996).  
[3] J. T. Farrar, *J. Phys. Oceanogr.* **38**, 1669 (2008).  
[4] T. Shinoda, *Sci. Online Lett. Atmos.* **6**, 17 (2010).  
[5] G. B. Whitham, *Linear and Nonlinear Waves* (Wiley-Interscience, New York, 1974).  
[6] W. C. Elmore and M. A. Heald, *Physics of Waves* (Courier Dover, New York, 2012).  
[7] H. J. Pain, *The Physics of Vibrations and Waves* (John Wiley & sons, New York, 2005).  
[8] O. Bühler, N. Grisouard, and M. Holmes-Cerfon, *J. Fluid Mech.* **719**, R4 (2013).  
[9] E. Gagnaire-Renou, M. Benoit, and P. Forget, *J. Geophys. Res.* **115**, C12058 (2010).  
[10] C. J. Huang and F. Qiao, *J. Geophys. Res.* **115**, C04026 (2010).  
[11] T. Tanimoto, *Geophys. J. Int.* **168**, 571 (2007).  
[12] R. K. Scott and L. M. Polvani, *J. Atmos. Sci.* **64**, 3158 (2007).  
[13] W.-S. Lu, *Theor. Appl. Climatol.* **55**, 221 (1996).  
[14] S. D. Zhang and F. Yi, *J. Geophys. Res.* **107**, 4222 (2002).  
[15] E. Fermi, J. Pasta, and S. Ulam, Los Alamos Report No. LA-1940, 1955, p. 978, reprinted in *Collected Papers of Enrico Fermi* (University of Chicago Press, Chicago, 1965), Vol. II, p. 978.  
[16] V. I. Arnol'd, *Russ. Math. Surv.* **18**, 9 (1963).  
[17] J. Ford, *Phys. Rep.* **213**, 271 (1992).  
[18] F. M. Izrailev and B. V. Chirikov, *Sov. Phys. Dokl.* **11**, 30 (1966).  
[19] B. Gershgorin, Y. V. Lvov, and D. Cai, *Phys. Rev. E* **75**, 046603 (2007).

- [20] B. Gershgorin, Y. V. Lvov, and D. Cai, *Phys. Rev. Lett.* **95**, 264302 (2005).
- [21] W. Lee, G. Kovačič, and D. Cai, *Proc. Natl. Acad. Sci. USA* **110**, 3237 (2013).
- [22] Y. Wakata, *J. Oceanogr.* **63**, 483 (2007).
- [23] M. Wilczek and Y. Narita, *Phys. Rev. E* **86**, 066308 (2012).
- [24] C. Alabiso, M. Casartelli, and P. Marenzoni, *J. Stat. Phys.* **79**, 451 (1995).
- [25] W. Lee, Ph.D. thesis, New York University, 2009.
- [26] H. Mori, *Progr. Theor. Phys.* **33**, 423 (1965).
- [27] R. Zwanzig, *Nonequilibrium Statistical Mechanics* (Oxford University Press, Oxford, 2001).
- [28] A. J. Majda, D. W. McLaughlin, and E. G. Tabak, *J. Nonlinear Sci.* **7**, 9 (1997).
- [29] D. Cai, A. J. Majda, D. W. McLaughlin, and E. G. Tabak, *Physica D* **152**, 551 (2001).
- [30] W. Lee, G. Kovačič, and D. Cai, *Phys. Rev. Lett.* **103**, 024502 (2009).
- [31] V. E. Zakharov, V. S. L'vov, and G. Falkovich, *Kolmogorov Spectra of Turbulence* (Springer-Verlag, Berlin, 1992).
- [32] P. D. Miller, *Applied Asymptotic Analysis* (American Mathematical Society, Providence, 2006).
- [33] J. Kevorkian and J. D. Cole, *Multiple Scale and Singular Perturbation Methods* (Springer, New York, 1996).
- [34] A. Dhar, *Adv. Phys.* **57**, 457 (2008).
- [35] T. N. Shah and P. Gajjar, *Commun. Theor. Phys.* **59**, 361 (2013).
- [36] P. Poggi and S. Ruffo, *Physica D* **103**, 251 (1997).
- [37] T. Dauxois, S. Ruffo, and A. Torcini, *Phys. Rev. E* **56**, R6229 (1997).
- [38] C. Alabiso and M. Casartelli, *J. Phys. A* **34**, 1223 (2001).
- [39] S. Nazarenko, *Wave Turbulence* (Springer, Berlin, 2011).
- [40] G. Benettin, R. Livi, and A. Ponno, *J. Stat. Phys.* **135**, 873 (2009).
- [41] R. Kubo, *Rep. Prog. Phys.* **29**, 255 (1966).